Journal of Colloid and Interface Science 633 (2023) 132–141

Contents lists available at ScienceDirect

Journal of Colloid and Interface Science

journal homepage: www.elsevier.com/locate/jcis

Super-enhanced evaporation of droplets from porous coatings

Mohsen Hosseini, Alejandro Rodriguez, William A. Ducker *

Dept. of Chemical Engineering and Center for Soft Matter and Biological Physics, Virginia Tech, Blacksburg, VA 24061, USA

GRAPHICAL ABSTRACT

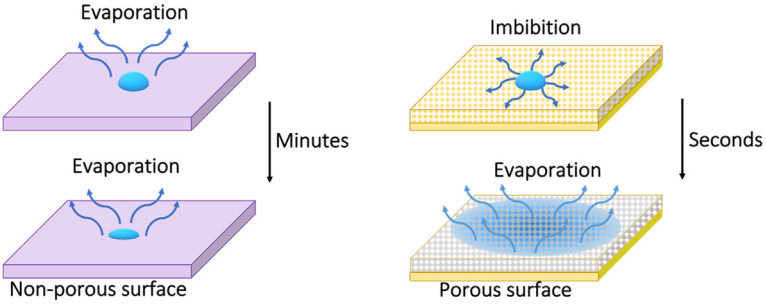

ARTICLE INFO

Article history:
Received 31 July 2022
Revised 8 November 2022
Accepted 12 November 2022
Available online 19 November 2022

Keywords:
Droplet
Evaporation
Imbibition
Porous
Coating

ABSTRACT

Hypothesis: The addition of a thin, hydrophilic, porous, coating to an impermeable solid will lead to more rapid evaporation of liquid droplets that impinge on the solid. The droplet will imbibe quickly, but the progress normal to the interface will be limited to the thickness of the coating, and therefore the liquid will spread laterally into a broad disk to expose a large liquid–vapor interface for evaporation.
Experiments: Liquid droplets of volume 2.5–25 μL were placed on solids and then both the mass and area of each droplet were monitored over time. We compared data for smooth, impermeable hydrophilic glass to the same glass that was coated in thin (35–109 μm) porous, hydrophilic-glass layer fabricated from glass beads.
Findings: The droplet was imbibed (wicked) into the coating within seconds, and the liquid spread laterally to form a thin, broad, disk. Critically, evaporation of a droplet was enhanced by a factor of 7–8 on the thin coating. The evaporation rate was not proportional to the reciprocal thickness of the coating. The ability to enhance evaporation of small droplets on a solid may have practical applications, for example, in speeding the death of microbes.

1. Introduction

Evaporation is important in a diverse range of applications, including removal of solvent to purify solutes, removal of solutes that were used to deliver dissolved substances (e.g. in printing), in cooling [1,2], in renewable energy schemes [3], and in drying surfaces. For example, evaporation plays a crucial role in inkjet printing, and it is responsible for "solidifying" the ink on the printing substrate [4]. Poor ink evaporation can result in smears and smudges, poor resolution, and quality issues [4]. Textiles are designed to dry quickly for moisture control [5]. After noting that drying can reduce the lifetime of microbial pathogens,[6] we are interested in materials that enhance evaporation of contaminated droplets on surfaces. More rapid drying could potentially speed the inactivation of the pathogens and thereby reduce the spread of disease [6–8]. Thin film evaporation has other important appli-

* Corresponding author.
E-mail addresses: mohsenhosseini@vt.edu (M. Hosseini), alejandroar@vt.edu (A. Rodriguez), wducker@vt.edu (W.A. Ducker).

https://doi.org/10.1016/j.jcis.2022.11.065
0021-9797/

cations in heat pipes [9], electronics [10], and spray cooling [11]. Many other processes that depend on evaporation can be improved by increasing the rate of evaporation.

Evaporation of large volumes (dimension ≫ mm) of water at surfaces is accelerated by gravity, which pulls macroscopic liquids down into disc-shaped objects (puddles) on solids, and thereby spreads the liquid into a large area that hastens evaporation. At low Bond number, gravity does not do us this service, and liquids are forced by surface tension to sit up in spherical-cap-shaped droplets that minimize the surface area and slow evaporation. Here we examine a solution to this problem that spreads out droplets and facilitates evaporation.

We investigate the increase in rate of evaporation of aqueous droplets that arises when a thin porous surface coating on a hydrophilic solid imbibes (wicks) the liquid into the porosity. Because the porous coating is thin and the underlying solid is hydrophilic, imbibed liquid is forced to spread laterally near the surface, causing a large increase in liquid–vapor area and a rapid increase in evaporation (Fig. 1).

The terminology for describing porosity can be confusing and we will use the literal meaning that pores with dimensions greater than 1 μm are micropores whereas pores with dimensions less than 1 μm are nanopores. Prior work on evaporation from bulk porous materials shows a very *slow* rate of evaporation due to the liquid transport into the interior of the porosity [12]. In addition, there has been some prior work on thin porous materials which we now describe. Unno et al. [13] increased the evaporation rate of a water droplet on a heated surface by a factor of 1.2 through the addition of a nanoporous coating. Gimenez et al. [14] demonstrated that a nanoporous film also increased the evaporation rate of a 1 μL water droplet by a similar factor of 1.2 due to the formation of a wetted annulus region surrounding the bulk fluid. They found that increasing the salt concentration of the water droplet as well as decreasing the temperature of the ambient air increased the wetted annulus area by reducing the surface tension, thereby increasing the rate of evaporation [14]. In previous work from our group, we reported an enhancement by a factor of about 3 for evaporation of water from a microporous hydrophilic coating [7]. Very recently, Gonçalves et al. [15] demonstrated that water droplets on porous fabrics increased the rate of evaporation by a factor of 2.6 compared to a nonporous flat substrate. Previously Oko et al. studied evaporation from thick porous materials [16,17] and did not observe enhanced evaporation rates compared to non-porous materials [16]. Certain applications have already begun to incorporate porous films as a method of optimizing evaporation, such as solar evaporation [18].

Several authors have investigated evaporation of water near its boiling point. Goh et al. [19] was able to increase the rate of evaporation of an 8 μL water droplet by a factor of 3.8 through the use of surface modified graphene nanoplatelets (GNPs) at a surface temperature of 95 °C. This investigation was continued by Tong et al. [20], who also demonstrated elevated evaporation rates of a graphene-oxide (GO) deposited film over a two-phase closed thermosyphon. Upon application of a 2 μL water droplet over the coating, it would wet a large portion of the surface area and therefore amplify the rate of evaporation by a factor of 4 at a surface temperature of 130 °C [19]. In related work, there is an effort to increase heat transfer by enhancing evaporation with structured surfaces [21,22], particularly for electronics [21].

Evaporation rates can also be altered by changing the liquid phase. For example, Nguyen et al. [23], demonstrated that addition of nanoparticles to a sessile droplet increased the rate of evaporation. They observed that nanoparticles would accumulate at the leading edge of the droplet due to the coffee-ring effect, causing pinning of the three-phase line during subsequent evaporation. Pinning the three phase line maintains a large area of air–vapor interface, thereby increasing the overall rate of evaporation [23].

Evaporation of a droplet from a thin porous coating is fundamentally different than evaporation from a flat surface. When a droplet is placed on a porous coating, there are two time periods: the time for imbibition and the time for evaporation. If imbibition is prohibited by a high contact angle or by lack of connectivity to the surface, then porosity will be irrelevant. The rate of imbibition needs to be at least the same order as evaporation to gain potential advantages from imbibition. As a first approximation for the imbibition time into a porous solid, t_I, it is common to use a model of a single straight cylindrical pore, which results in the Washburn Equation [15]:

$$t_I = \frac{2\eta}{\gamma r_p \cos\theta} L^2 \tag{1}$$

where η is the liquid viscosity, γ is the vapor–liquid interfacial tension, r_p is the radius of the pore, θ is the contact angle of liquid on the non-porous solid, and L is the distance travelled. More sophisticated treatments include the extra distance that a liquid must travel due to tortuosity of the film, but depend on similar parameters as well as the void fraction, shape geometry and pore size distribution [24–27]. Using the Washburn equation, we see that more rapid imbibition arises from a lower liquid contact angle, a thinner coating, and importantly, a larger pore size. For this reason, the current work investigates hydrophilic glass coatings that were fabricated from 3 to 10 μm diameter particles to obtain hydrophilic micropores and therefore rapid imbibition. Clearly nanopores would provide slower imbibition, which could lessen evaporation rate effects that are due to imbibition.

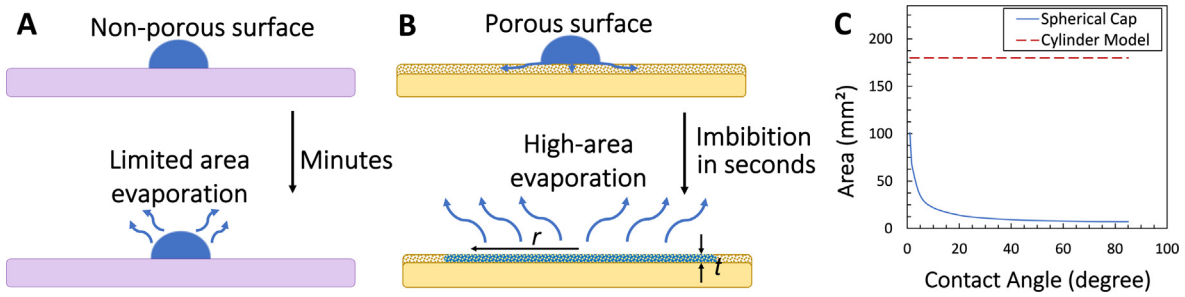

Fig. 1. (A) Schematic of evaporation of a droplet on a flat sample. The droplet has a small area and slow evaporation. (B) Schematic of evaporation on a thin, porous, hydrophilic coating. The droplet is imbibed into the porous coating and spreads over a large area in seconds. The large area causes more rapid evaporation than on the non-porous surface. The figure is not to scale; the drop radius is of order millimeters whereas the coating is at most 0.1 mm thick. (C) Calculated solid–liquid surface areas of droplets for the cases in (A) and (B). For the drop on the non-porous surface, we assumed a spherical cap, and for the imbibed liquid, we used a model of a cylindrical disk of thickness 35 μm to approximate the imbibed liquid. The droplet volume is 2.5 μL in both cases.

Intuitively, one might expect that evaporation depends somehow on both the area of the vapor–liquid interface [13–15,19] and on the gradient of chemical potential between liquid in the pores and the bulk vapor above the pores. However, in their work on droplet evaporation from an impermeable solid via diffusion, Hu and Larson [28] showed that the rate of evaporation of droplets on impermeable solids is not homogenous with radial position: evaporation is greater near the three-phase line of a simple droplet. They derived an equation showing that the evaporation is proportional to the droplet contact radius, R:

$$\text{Evaporation Rate} = \pi RD(1-H)c_v(0.27\theta^2 + 1.3) \quad (2)$$

where D is the vapor diffusivity, H is the relative humidity, c_v is the saturated vapor concentration, θ is the contact angle of a droplet on an impermeable solid, and the last term in parenthesis is an empirical fit.

To accelerate the evaporation, we employ *thin* porous hydrophilic coatings. When droplets are placed on such a coating, the liquid is rapidly imbibed and reaches the bottom of the coating. If the underlying solid is impermeable and hydrophilic, the liquid then spreads radially and causes a thin film near the solid (Fig. 1). Restriction of the liquid to a thin film has two consequences: (1) For a constant volume, it causes the liquid from the droplet to spread over a large area, producing a large vapor–liquid interfacial area (see Fig. 1B). Since evaporation occurs at the vapor–liquid interface, spreading is advantageous for evaporation. (2) Proximity to the surface of the coating aids evaporation by providing a higher gradient ofchemical potential. For example, if there were to be a thick layer of vapor between the imbibed liquid and the vapor, there could be a gradual gradient in partial pressure of vapor [28].

To obtain a large area when the gravitational force is weak (low Bond number), we need wettable porosity and the limit of large $\sqrt[3]{V/\varepsilon}/t$, where, V is the volume of the droplet, t is the thickness of the porous coating and ε is the pore space volume fraction. We define the normalized length, $\hat{l} = \sqrt[3]{V/\varepsilon}/t$ that describes the radius of the droplet if it were to form a cylindrical disk spanning the thickness of the porosity.

We now consider the simplistic model of the liquid in the porous film as a cylindrical disk (Fig. 1B). Forcing the droplet into a very small thickness results in a large liquid–vapor interface. For example, a 2.5 μL droplet in a 35-μm-thick disk has an area of about 180 mm^2. For a spherical cap, for comparison, even a contact angle of 1° only has an area of about 100 mm^2. Our experience is that such a low angle is very difficult to maintain in a practical environment due to contamination. Even very hydrophilic glass rapidly assumes an angle of at least 30° when sitting in air in our lab., in which case the droplet air-vapor interface would only be about 11 mm^2, i.e., about 17× lower than for a cylindrical model. Yet the rate of imbibition is only slightly diminished by a 30° contact angle (See equation). Thus, a thin porous coating forces a droplet to have a large surface area, which is relatively insensitive to the contact angle, when the angle is low. Fig. 1C compares the vapor–liquid surface areas of droplets on smooth and thin porous surfaces.

Deegan et al. [29] suggested the following the following equation to calculate the flux of evaporation from a droplet with complete wetting:

$$\left(\vec{J}.\vec{n}\right) = J_o\left(1-\left(\frac{r}{R}\right)^2\right)^{-0.5} \quad (3)$$

where $\vec{J}$ is the local flux of evaporation, $\vec{n}$ is the normal vector, J_o is the flux of evaporation in the center of the droplet, and r is the local radius and R is the total radius of the droplet. Staring from Deegan's equation, we obtained the evaporation rate for the limit of zero contact angle and large area ($\hat{l} \gg 1$) that are the conditions rapid evaporation from liquid imbibed into a porous coating (See Supplementary Material, Evaporation from a porous coating). The vapor above the droplet is in quasi-steady state because of the separated times scales: normal evaporation (10^{-5} s) < equilibration across the droplet (1 s) < imbibition (20 s) < evaporation total time (200 s). Hence:

$$\text{Evaporation Rate} = \pi\frac{R^2}{d}D(1-H)c_v \quad (4)$$

where d is a characteristic distance for the evaporation from the porous surface. Here R is the radius of the drop within the porosity. We, therefore, expect the evaporation rate to be proportional to the wetted area of the imbibed disk of liquid in the limit of low Bond number and large $\hat{l}$. This result is intuitively reasonable: for a large area, the faster evaporation that occurs at the perimeter of the droplet has less influence on the total evaporation, and the evaporation is proportional to the area.

We note an additional advantage of large pore sizes. In addition to slowing imbibition, smaller pore sizes may also retard evaporation by lowering the vapor pressure adjacent to imbibed liquid. The Kelvin equation describes the equilibrium vapor pressure above a curved meniscus,p_r

$$p_r = p_\infty \exp\left(\frac{2\gamma V_L}{r_{vl}RT}\right) \quad (5)$$

where p_∞ is the equilibrium vapor pressure above a flat interface, V_L is the molar volume of the liquid, r_{vl} is the radius of curvature, γ is the surface tension, R is the gas constant, and T is the temperature. For the situation considered here, where $\theta < 90°$, r_{vl} is negative, so evaporation is retarded from menisci compared to a flat surface. This effect increases for smaller radii but is unimportant for radii greater than about 1 μm.

We have three goals in this work: (1) to demonstrate rapid evaporation of water from a porous coating, (2) to examine the effect of coating's thickness and (3) to investigate the relationship between wetted area and rate of evaporation. Our coatings are fabricated from spherical glass particles with diameter 3–10 μm. We examined thin coatings (35–109 μm thickness), rather than porous solids, so that the droplet would spread in the plane of the surface and thereby force a large vapor–liquid interface. We varied the thickness to examine the relationship between the spread of the droplet and the rate of evaporation. The spread was monitored by video and the rate of evaporation was monitored by weighing the droplet (See Schematic in Figure S1). All experiments were conducted at a constant temperature of 25 °C and with a constant relative humidity (RH) of 33 %.

The experimental results show a much higher rate of liquid evaporation when a droplet is placed on a porous coating compared to a non-porous solid. Interestingly, the evaporation rate from porous coatings is not proportional to the measured droplet area or the reciprocal coating thickness, although it does increase with decreasingcoating thickness.

2. Materials and methods

2.1. Materials

100 % Ethanol (ACS grade), 70 % ethanol (Reagent Grade), sodium hydroxide beads (NaOH, ACS grade), nitric acid (HNO_3 70 %, ACS grade) and glass slides (25 × 75 × 1 mm) were purchased from VWR. Glass beads (size range 3–10 μm) were obtained from Corpuscular (NY, USA). Trimethylchlorosilane (TMCS 98 %) was purchased from Fisher Scientific. Magnesium chloride ($MgCl_2$

anhydrous, purity ≥ 98 %) was obtained from Sigma-Aldrich. Water was purified using a Milli-Q Reference system (MilliporeSigma). The glass slides and particles are both soda lime glass and have very similar chemistry (Table S1).

2.2. Fabrication of porous coatings

Glass slides were initially cut into 20 mm × 20 mm pieces and then rinsed with water and ethanol. Porous glass coatings were prepared by depositing suspensions of glass beads in ethanol on the glass slides followed by a heat treatment to cause partial sintering. Variation in thickness of porous coating was achieved by varying the mass fraction of spheres in the suspension. Five different suspensions (6.2, 9.3, 12.4, 15.5 and 18.6 wt%) were prepared and sonicated for 10 min. 375 μL of the suspension was then drop-casted on glass pieces and left in room temperature to dry for 30 min. Samples were then placed in a furnace at room temperature and then the temperature was increased to 615 °C over a period of 25 min. After two hours of heat treatment at 615 °C, the furnace was switched off and samples were cooled overnight. The heat-treated samples were rinsed with water and dried using a stream of nitrogen.

2.3. Deposition of TMCS on surfaces

Hydrophobic coatings were prepared by deposition of vapor-phase TMCS on porous coatings or flat glass. Samples were plasma cleaned with oxygen at less than 200 mTorr at 100 W power for 5 min and then placed in a sealed glass container for 24 h with a beaker of liquid TCMS and molecular sieves. Molecular sieves were used to reduce the pressure of water vapor. Next, samples were sonicated in ethanol for one minute (to remove loosely bound TMCS) and dried with a stream of nitrogen. The advancing and receding contact angles were 97°±2° and 74°±2° respectively for flat glass surfaces and 106°±3° and 79°±4° respectively for porous glass coatings.

2.4. Characterization of microparticles and coatings

The coating thickness, the extent of sintering and the coating structure were determined by Scanning Electron Microscopy (SEM, JEOL JSM-IT500). Examples of SEM images of the porous films with different thicknesses are shown in Fig. 2; further images showing porosity and the necks caused by partial sintering are in Supplementary Material Figure S2. The pores appear to be smaller at the top surface. The thicknesses of the films were 35 ± 3 μm, 46 ± 1 μm, 63 ± 1 μm, 79 ± 1 μm and 109 ± 3 μm. X-ray Photoelectron spectroscopy (XPS, PHI VersaProbe III, Al Kα monochromatic, Analysis Area: 1000 μm × 200 μm) showed a similar surface elemental composition of flat and porous samples (Table S1). The pore volume fraction was 41 ± 4 % as determined by measurement of the spread area of the droplet as described previously [30]. The particles are large and the coating is thin so the internal surface area of the pores is too small to be resolved by BET. From a combination of the known mass of particles deposited, assuming average particle diameter of 8 μm, and the particle volume fraction, we estimate a surface area of 0.4 m^2 per gram of coating.

2.5. Evaporation apparatus

Figure S1 (Supplementary Material) shows a schematic of our custom-build apparatus to study the rate of evaporation from porous surfaces. Supplementary Material Figure S1 contains a photograph and further details of the apparatus. The heart of this apparatus was an analytical balance (Denver Instrument, model M−220D) to measure the mass of a droplet as a function of time since deposition on the porous coating within an enclosed chamber. The balance can be read to 0.1 mg. The mass was recorded every 1 s on a computer using Winwedge (Taltech, USA) software. The temperature within the enclosure was maintained at 25.2 ± 0.2 °C using 6 polyimide heaters (Omega Engineering, model KHA-108/10) and a feedback controller (Elitech STC-1000Pro). The relative humidity was maintained at 33.1 ± 0.6 % with 40 mL of saturated aqueous magnesium chloride salt in a container within the enclosure. The masses of the various water phases are 40 g in the liquid reservoir, 5–25 mg in the droplet at start, and about 150 mg in the vapor. Video (30 fps) of the droplet was obtained from a camera placed about 9 cm above the sample. There was no forced air movement during the experiment. The temperature and relative humidity (RH) of the environment were measured using probes installed within 4 cm of the sample. Thus, the mass, video, temperature and RH were all recorded with time. The chamber was closed and the contents were allowed to reach equilibrium, which usually took about greater than 6 h, before a micropipette was used to place droplets on samples. Supplementary Material S3 contains examples of the time course of temperature and humidity changes and estimates of evaporation effects on the sample temperature. After a droplet was placed on the solid, there was a perturbation on the balance from the falling drop followed by a longer period (about 20 s) of fluctuation due to the movement then withdrawal of our hand from the glove within the sealed chamber. For this reason, data shown in figures starts 20 s after a droplet was placed on the surface. Supplementary Material contains a calculation showing that the thin film temperature decreases by only 0.2 °C during steady state evaporation.

2.6. Statistical treatment

Our default was to have three independent measurements of each sample, i.e., use of three different porous coatings for each condition. The error bars in figures refer to the standard deviation for the three replicates and "±" in the text refers to the 95 % confidence interval. Because of the long time for the chamber to reach equilibrium, we found it convenient to measure results for all three drop volumes on the same sample in series, with a pause of at least 40 min after the previous drop had evaporated. The validity of this method is examined in Supplementary Material, Fig. S4. A *p*-value near or below 0.05 was a necessary condition for a quantitative conclusion.

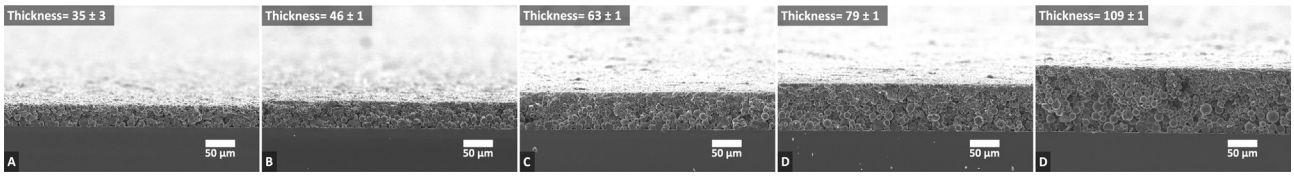

Fig. 2. SEM images of porous coatings with thickness labelled. Images show uniform thickness of coatings.

3. Results and discussion

3.1. Droplet evaporation is much faster on a thin porous coating

The addition of a porous hydrophilic coating dramatically increased the rate of evaporation of water from a droplet (Fig. 3). The evaporation of a 5 μL droplet from a 35-μm-thick porous glass coating is 8 times more rapid than on uncoated, non-porous glass, and 37 times more rapid than on the bulk porous glass prepared using the same glass beads. The very large increase in evaporation on a coated surface is the principal conclusion of this work and is likely to be of practical use.

We investigated a variety of droplet sizes and coating thicknesses in the limit of small Bond number and $\widehat{l} = \sqrt[3]{V/\varepsilon}/t \gtrsim 10$. The evaporation rates, shown in Fig. 4, demonstrate that evaporation is much larger for all coatings for all drop sizes. The coating increased evaporation compared to the uncoated surface by a factor of 6.8 for a 2.5 μL droplet, 7.8 for a 3.5 μL droplet, 8.0 for a 5 μL droplet, 7.7 for a 10 μL droplet, and 6.2 for a 25 μL droplet. Note that the (large) 25 μL droplet spread to the edge of the sample for all coatings, which may have limited evaporation for that droplet volume.

Our explanation of the evaporation increase is based on imbibition. To test this, we hydrophobized a 63-μm thick porous glass coating by depositing TMCS on the surface of the pores and also a flat glass surface to use as a control, and measured the evaporation of a 5 μL droplet. The advancing contact angle on the porous coating was 106°±3°, so we did not expect imbibition and none was observed during the period of drying (Figure S5). The rate of evaporation of a 5 μL droplet on a flat hydrophobic surface was 2.7 μg/s and on the porous hydrophobic coating was 2.6 μg/s respectively. That is, the difference was negligible when comparing hydrophobic surfaces. This is consistent with the idea that imbibition is necessary for the enhanced rate of evaporation. Compared to the hydrophilic glass, the addition of the hydrophobic porous coating decreased the rate of evaporation.

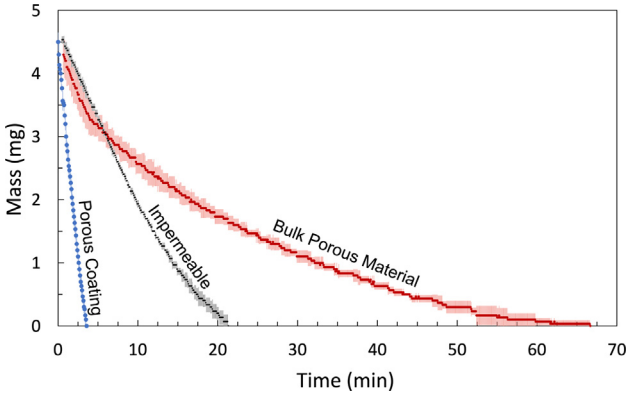

Fig. 3. Effect of porous glass coating on the rate of evaporation of a 5 μL water droplet from glass. Results from three samples are shown: (1) impermeable glass, (2) impermeable glass with a 35-μm-thick porous glass coating, and (3) a 5-mm thick sample fabricated entirely of porous glass. For the thick sample, there is a change in rate at about 6 min that occurs when the liquid loses contact with the top of the sample. Photographs of the droplet on the thick porous coating are in Figure S10. Points show the average mass for three measurements and the shaded area is the standard deviation. Addition of the thin porous coating speeds evaporation by a factor of 8 compared to the impermeable glass, and by a factor of 37 compared to the bulk porous material.

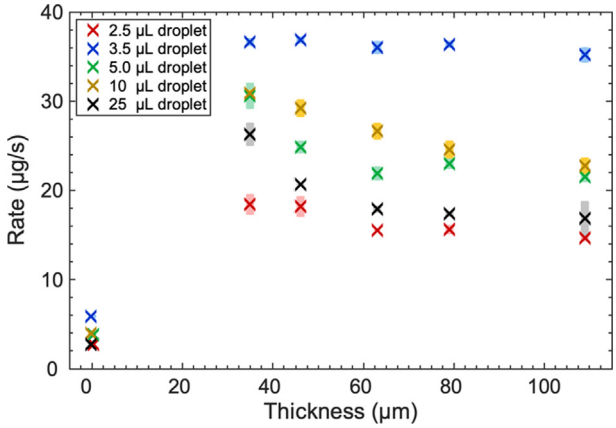

Fig. 4. Effect of porous glass coating on the rate of evaporation of water from glass. The rate was obtained from the slope of mass vs time, an example of which is shown in Fig. 6. The rate of evaporation is much greater for all the porous coatings than for the uncoated solid, which is plotted as zero thickness. ($p = 6 \times 10^{-34}$ Student's *t*-test, one tailed, heteroscedastic). Some of the zero-thickness data has been shifted slightly off zero for better visibility. Shaded areas indicate standard deviation of three independent experiments and "×" shows the average values. Faster evaporation occurs for droplets of greater volume because of their larger area, and there is a decrease in evaporation with coating thickness.

3.2. Imbibition leads to a Large-Area droplet within seconds

The progress of imbibition was monitored by video. Imbibition always began immediately when the droplet was placed on the coating, and lead to a rapid radial spread of the droplet within the coating from the point of impact. After a short time (typically 20 s), the radial spread reached a maximum where there was a dwell before the droplet area decreased (See Fig. 5).

We examined 5 droplet volumes: 2.5 μL, 3.5 μL, 5 μL, 10 μL and 25 μL. The 2.5 μL and 3.5 μL droplets were designed so that, even for the thinnest coating, the imbibed droplet did not reach the edge of the porous coating, and, for the 5 μL droplet, the imbibed liquid only reached the edge for the thinnest coating. The 25 μL droplet was chosen such that the coating void capacity would be insufficient, and in practice the imbibed droplet reached the edge of the coating, and hence adopted a non-circular shape. Cases where the droplet reached the edge (coatings with thickness less than 46 μm for 5 μL droplets and all coatings for 10 μL and 25 μL droplets) are not discussed in subsequent sections because the behavior of the droplet was affected by the imposition of the edges, which was a side-effect of the sample size of 20 mm × 20 mm. In all cases, the radius of imbibition inferred from the optical images was much greater than the contact radius of the same drop size on an impermeable solid. This large radius was achieved within 20 s on porous coatings, which was much less than the total evaporation time (100 – 200 s). This means that the majority of evaporation time occurs after there is a large-area droplet within the coating. For comparison, in prior work where nanoporous silica thin films were examined, imbibition was slower and limited to a smaller area around the droplet. As a result, only a 10 % increase in evaporation was observed for a 5 μL droplet on nanoporous silica coatings [14].

3.3. The evaporation rate is approximately constant

The mass of the droplet diminished approximately linearly with time for all combinations of drop volume and coating thickness, i.e. the rate of evaporation is constant. Data for a 2.5 μL water droplet on a 35-μm porous coating and 5 μL water droplet on a 109-μm porous coating are shown in Fig. 6; other examples are in Figure S6.

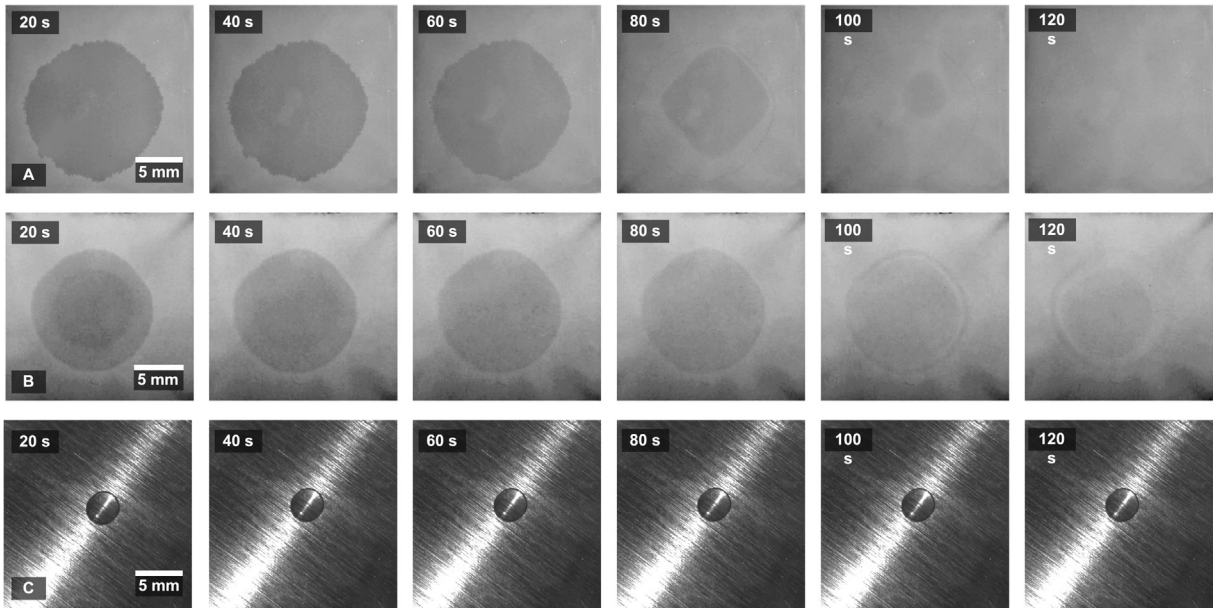

Fig. 5. Time lapse photographs showing evaporation of a 2.5 μL droplet on three different solids. The images are in reflection, and the reflectivity is diminished in the wetted area because of reduced scattering when the air is replaced by higher index water in the pores. (A) 35 μm-thick porous coating. (B) 109 μm-thick porous coating. (C) Non-porous glass. Scratch marks are due to steel under the glass.

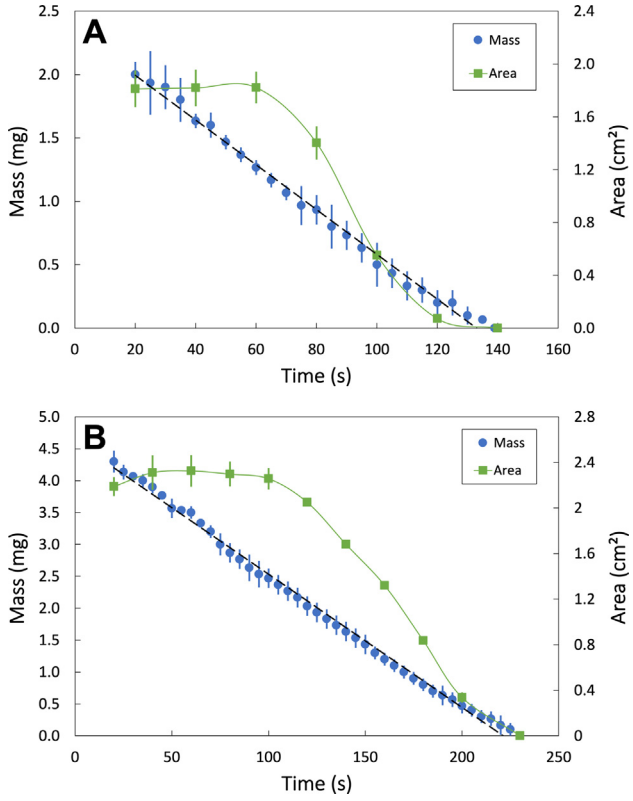

Fig. 6. Time course of mass and area of (A) a 2.5 μL water droplet on a 35-μm thick porous glass coating and (B) a 5 μL water droplet on a 109-μm thick porous glass coating. Error bars show the standard deviation of three independent measurements on independent samples. The black dashed line is a fit to the mass data between 20 s and 140 s for (A), and between 20 s and 220 s for (B), and indicates that the evaporation rate is approximately constant in this period (The linear regression slope for (A) is $-0.0184 \pm 6 \times 10^{-4}$, $R^2 = 0.992$ and for (B) is $-0.0209 \pm 4 \times 10^{-4}$, $R^2 = 0.996$). The area of minimum light intensity (maximum wetting) remains constant for about the first 60 s in (A) and first 100 s in (B) and then diminishes. The curved line is an aid to the eye for the area measurements. The surface area was obtained from the optical image using ImageJ software.

Recall that the readability of the balance is only 0.1 mg so we cannot clearly resolve changes in mass at the end of the evaporation period. The dark area within the coating grows very rapidly, then remains almost constant for a period time, and finally diminishes until evaporation is complete (Fig. 6). This effect is discussed in more detail in Section 3.5, and occurs for all droplet sizes and coating thicknesses. We note that our use of the term "area" or "wetted area" denotes the dark area that is continuous in the images. The video does not resolve the individual particles in the coating or the shape of liquid menisci, so the reported area is simply the cross-sectional area including both wetted particles and water. Careful viewing of, for example, Fig. 5B at 120 s, reveals that there is a dark ring beyond the continuous disk. Given that the evaporation rate is constant over almost the entire period of evaporation, a reasonable hypothesis is that water remains over the entire cross-sectional area that was initially wetted. The images are in reflection, and the dark area is due to a better match in refractive index in the porosity compared to the silica, i.e., water rather than air. But if there is air at the surface of the porosity, there would still be scattering at the surface and we may not see water below. So, the constant evaporation rate is consistent with the idea that some water remains at the perimeter for the entire course of evaporation, but the optical images suggest that the droplet becomes inhomogeneous in thickness. Because ($R_{initial}$ / t) is so extreme, variation in thickness over time may not affect the area available for evaporation at the liquid–vapor interface.

3.4. The thickness of the coating affects the rate of evaporation

We hypothesized that, in the presence of a coating, a thinner coating would cause faster evaporation. The basis of this hypothesis was that a thinner coating would cause the droplet to spread over a greater area, resulting in a greater liquid–vapor interface, which is the location of evaporation. Our model for this hypothesis was that the imbibed liquid would very rapidly form a cylindrical disk within the coating, and that the top, circular, area would be available for evaporation (Fig. 1B). Since the top, circular area of a cylindrical disk is the volume divided by the height, the area

for evaporation would be proportional to the reciprocal of coating thickness, t. Examining our model for 2.5 μL, 3.5 μL and 5 μL droplets in Fig. 4 (excluding droplets that reached the edge of the solid), the data qualitatively supports the hypothesis: the evaporation rate does diminish with thickness, t. But quantitatively, the rate is not proportional to $1/t$. Linear regression with two factors, $1/t$, and the droplet size, V_d, (R^2 = 0.84), gives:

$$\text{Rate} = 2.89 \cdot V_d + \frac{330}{t} + 3.62 \quad (6)$$

Where Rate is in μg/s, V_d in μL and t in μm. The reciprocal coating thickness ($p = 2 \times 10^{-11}$), the droplet size ($p = 2.3 \times 10^{-15}$) and the constant were significant ($p = 2 \times 10^{-3}$). The trend of a higher rate for a larger volume is understandable that there is simply more area for a more voluminous droplet. Quantitatively, the dependence of evaporation on reciprocal thickness is not what the cylindrical disk model predicts. The evaporation rate increases with $1/t$ (Eq. (6) and Figure S7) but there is a large constant term in Eq (6), 3.6 ± 2.2: the rate is not proportional to $1/t$. The origin of this phenomenon is clear from Fig. 7, which plots the measured plateau droplet area and the area from the cylinder model as a function of reciprocal coating thickness. The measured area is a much weaker function of reciprocal coating thickness than predicted by the cylinder model: for the thicker films, the actual area is much greater than for the cylinder model. This may simply be that in the thicker films, our microscopy does not resolve water at greater r if it is not at the surface of the porosity. The existence of variable water thickness means that we cannot determine the area from the cylinder model using the droplet volume, coating thickness and porosity (Fig. 8).

3.5. Balance between the rate of evaporation and imbibition

The simple cylinder model of the liquid within the porous coating is inconsistent with the measured area for different thicknesses and the observed constant rate of evaporation. After a droplet landed on a porous coating, it was imbibed within seconds, spread radially, and reached a maximum area within about 20 s. A constant apparent area was then maintined for about 40-100 s all thicknesses and droplet volumes (Fig. 8). The capillary length of water is about 2.6 mm, which is much greater than the coating thickness, so after imbibition, hydrostatic pressure is unimportant compared to the pressure from surface tension. In the porous coating, the Bond number is about 10^{-3}; and the capillary number is about 10^{-5} during the initial imbibition, but is subsequently much smaller, so viscous effects are unimportant during most of the period of evaporation.

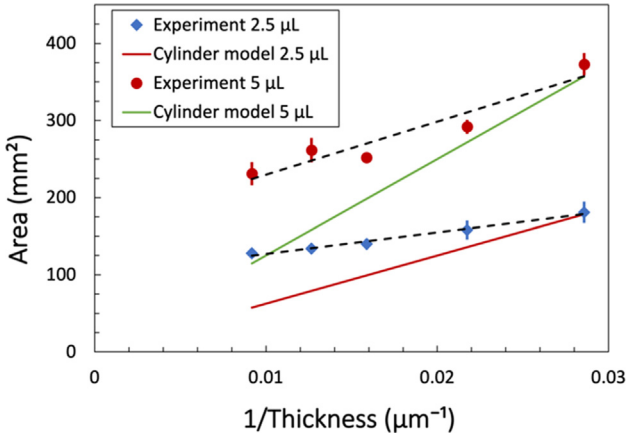

Fig. 7. Comparison of measured area and the area of a cylindrical disk for two drop volumes: 2.5 μL and 5 μL.

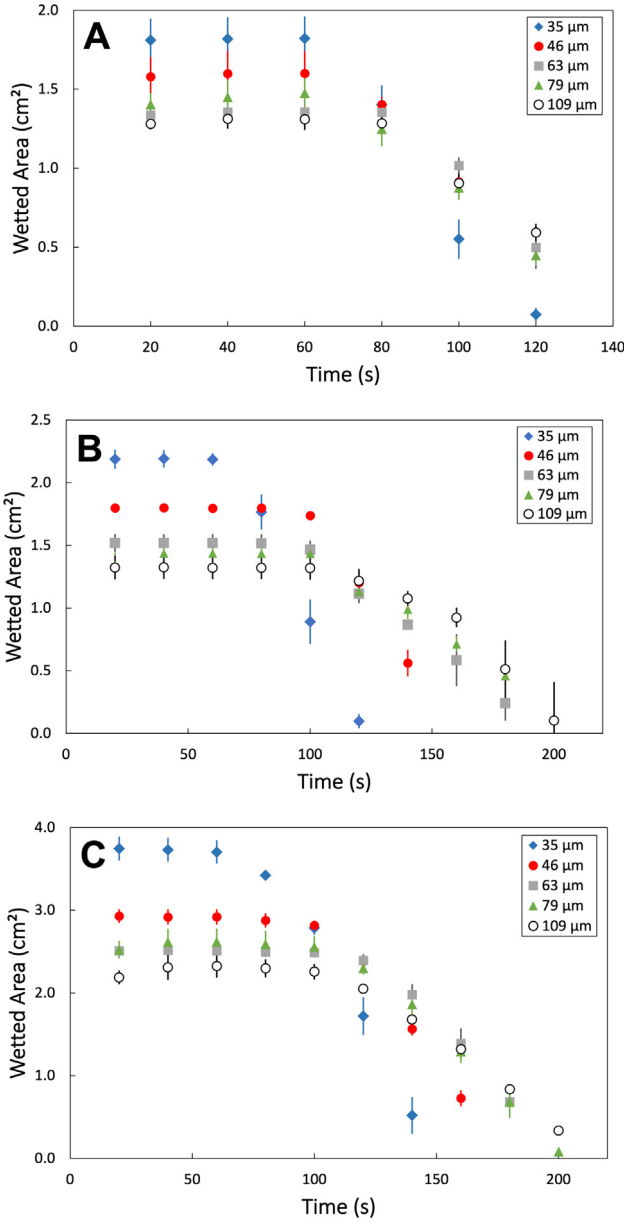

Fig. 8. The wetted area of water droplets on porous samples with different thicknesses. (A) 2.5 μL droplet. (B) 3.5 μL droplet. (C) 5 μL droplet.

The plateau in measured area during evaporation must correspond to a reduction in average thickness of the water film, and some images show that this thinner area is near the circumference (Fig. 5B, 20 s). The plateau area is likely the effect of the opposite dependences of evaporation and imbibition on radial distance. The greater the spread of the droplet, the greater the surface area of available liquid–vapor interface for evaporation and the greater the radial distance for imbibition, thereby slowing the feed. At some point radial imbibition cannot keep up with evaporation at the circumference, and advance of the droplet halts. The evaporation rate remains constant in the constant area regime because of the balance between evaporation and imbibition that keeps the area constant. It appears that this balance is reached very early in our experiments.

At this point, we reiterate an important point made by Hu and Larson [28] that the rate of evaporation on impermeable solids is

not homogenous with radial position: evaporation is greater near the three-phase line of a simple droplet. Qualitatively, we would also expect that evaporation would be greater at the perimeter of an imbibed droplet (maximum r): in the center of the droplet the diffusion is essentially 1-D whereas, near the perimeter, diffusion is 3-D. To test whether evaporation was dominant at the perimeter of imbibed droplets, we added blue dye to the test droplet prior to imbibition. During the course of evaporation, the dye became concentrated in a ring at the plateau perimeter (Figure S8). The formation of this "coffee ring" is consistent with advection of the dye to the perimeter line after imbibition, and thus with greater evaporation at the perimeter. It also shows that the perimeter is pinned for much of the period of evaporation. Since the perimeter grows with root area, if evaporation is dominant at the perimeter, the evaporation rate will grow more slowly than the area. Fast evaporation at the perimeter is also consistent with the observed thinning near the perimeter of the droplet.

To test the effect of evaporation on drop shape, we investigated the effect of slow evaporation by repeating an experiment at 90 % humidity instead of the 33 % used thus far. At 90 % humidity, the rate of evaporation was 3.4 times slower than at 33 % humidity but (a) optical images still showed variation in liquid thickness with radial distance and (b) the total area was not statistically different (Figure S9). This suggests that the drop shape and plateau area are strongly influenced by capillarity and not only evaporation.

3.6. The evaporation rate is linear in imbibition area in the limit of large $\hat{l} = \sqrt[3]{V/\varepsilon}/t$

In the limit of large $\hat{l}$, we expect the droplet to adopt a large area within the porosity, and therefore for the evaporation to be proportional to the area of the droplet as described in Equation (4). We tested this hypothesis using the measured plateau area. To test to the point of expected failure, we did additional measurements on solids with thicker, 360 μm-thick, coatings, where $\hat{l} < 5$ (open circles in Fig. 9). The data is shown in Fig. 9 where the data points

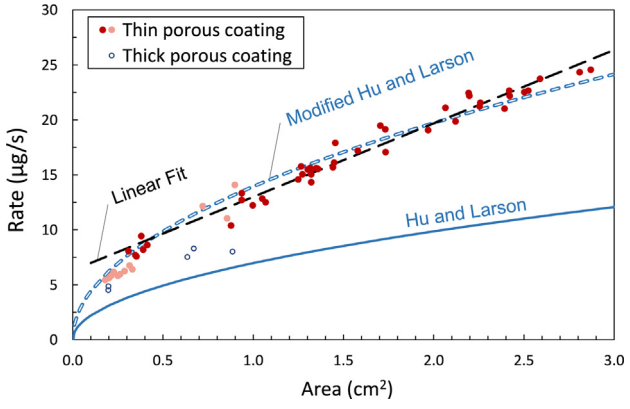

Fig. 9. The linear relationship between the rate of evaporation and the wetted area for large $\hat{l}$. The area was obtained from photography of the plateau area regime, and we only included data where the droplet never reached the edge of the sample. Data points are color-coded according to the value of $\hat{l} = \sqrt[3]{V/\varepsilon}/t$ (Red $\hat{l} \geq 20$, Pink $10 < \hat{l} < 20$, open circles $\hat{l} \leq 5$). The dashed black line is a linear fit to the data where $\hat{l} \geq 20$ (R^2 = 0.97). The blue lines are predictions from Hu and Larson's equation. The solid blue line is the rate of evaporation obtained by Hu and Larson's on impermeable solids (Equation (2)). The thick dashed blue line is a fit to Hu and Larson's equation for thin porous coatings ($t \leq 109$ μm) assuming that the contact angle is zero, and using the measured radius of the imbibed droplet (Equation (8), (R^2 = 0.97)). The five data points for the 350 μm-thick coatings are presented by open circles. (For interpretation of the references to color in this figure legend, the reader is referred to the web version of this article.)

are color-coded in bins of $\hat{l}$. For data where $\hat{l} > 20$, the data is clearly linear in area, R^2 = 0.97, and regression analysis gives the following rate equation:

$$\text{Rate} = 6.7 \cdot \text{Area} + 6.2 \tag{7}$$

where Rate is in μg/s and Area in cm^2. However, the rate is not proportional to the area because the intercept is far from zero. The 95 % confidence interval for intercept is 6.2 ± 0.6, so the area-dependence only accounts for about 50–80 % of the evaporation. The data for $\hat{l} < 20$ depart from the line, consistent with failure of Equation (4), as expected for an equation derived in the large-area limit. As the area becomes smaller, there is a larger percentage contribution from the perimeter, where evaporation is enhanced, and the data trends to a dependence on root area.

Hu and Larson's equation (Equation (2)) is also plotted on Fig. 9, where we assume that the effective contact angle is zero since the actual liquid shape is very flat. For a contact angle of 30°, the rate would only increase by 5 %. We further assume that the vapor diffusivity and humidity are the same as in bulk. The magnitude of evaporation is not well approximated by their equation for droplets on porous coatings.

Hu and Larson's equation includes an empirical factor, $(0.27\theta^2 + 1.3)$, which was obtained by comparison to finite-element modelling, and is equal to 1.3 for zero contact angle. Since this is an empirical factor for droplets on non-porous surfaces, which may not apply for liquid in a porous coating, we determined the value of the empirical factor for all our data on thin porous coatings (i.e., excluding the data for 350 μm coatings). This best fit (R^2 = 0.98) is:

$$\text{Evaporation Rate} = 2.6\pi RD(1 - H)c_v \tag{8}$$

That best-fit line is shown in Fig. 9 and gives a reasonable fit to data at all values of $\hat{l}$ that we measured, even for $\hat{l}$ as small as 9.8. The data for the 350-μm-thick sample is not close to the fitted line. For this thick film, the droplet may penetrate far from the surface and there may be additional resistance due to humidity in the pores above the liquid [28].

Finally, we note that the original Hu and Larson equation (Equation (2)) predicts the correct evaporation rate on the porous hydrophobic coating. The measured rate was 2.6 μg/s and prediction was 2.8 μg/s, and both values are similar to the hydrophobic flat with measured rate 2.7 μg/s and prediction 2.9 μg/s. The agreement for the hydrophobic porous coating is not surprising because, in this case, the droplet is not imbibed and therefore the situation is similar to a droplet on an impermeable solid. Evaporation via the vapor under the solid is not accounted for in Hu and Larson's model, but we expect this to be slow because of the long distances and small vapor gradients connecting the underside of the droplet to the bulk vapor.

4. Conclusions

The application of a thin, hydrophilic, porous coating to an impermeable solid caused droplets to spread on the surface and evaporate much more quickly than on the uncoated impermeable surface. Evaporation rates were up to 8 times greater on the porous coating than on the original uncoated solid at room temperature. Previous work has investigated nanoporous coatings, which typically increase the rate of evaporation by only about 1.2 times [13,14], presumably because of slow imbibition and low vapor pressure in the nanopores compared to micrometer-sized pores that were investigated here. Other prior work has investigated evaporation near the boiling point of water [19] or from bulk or thick porous materials (e.g. fabrics [15]). Work on (porous) paper

reports negligible increase in evaporation rate compared to flat surfaces [16] in contrast to the 8× increase observed here.

Our work demonstrates how to increase the rate of evaporation on impermeable materials by adding a thin permeable coating. As demonstrated here, the large, hydrophilic, pores allowed rapid imbibition, and the limited thickness of the coating forced the liquid to spread radially to form a large surface area disc for rapid evaporation. The drop then maintained a constant area for a large time period, despite ongoing evaporation. We used the non-dimensionalized droplet size, $\widehat{l} = \sqrt[3]{V/\varepsilon}/t$, as a measure of a thin film. For $\widehat{l} > 20$, the evaporation rate was linear in area. Hu and Larson's equation, which included empirical fits to data for droplets impermeable solids, was not a good fit to the rate data for droplets imbibed into porous coatings. However, we were able to obtain a good fit using the form of their equation but with a different empirical fit parameter.

In some cases, we resolved variable liquid thickness as function of radial distance from the center of the droplet. The existence of coffee ring demonstrated that evaporation was greater at the perimeter and that the liquid at the center was connected to the liquid at the perimeter. Future work could include scattering studies to determine the shape of the liquid within the coating.

Although the evaporation rate was greater for thinner films, neither the rate nor the droplet area was proportional to reciprocal thickness. Detailed modelling is needed to determine why the area remains constant and the thickness varies with radial position; an equation for the evaporation could be developed in terms of non-dimensionalized quantities. In future work, the effect of humidity, temperature, wettability, etc., on the kinetics of evaporation can be investigated.

We expect this method of accelerating the drying of solids could be used as a method of inactivating desiccation-sensitive pathogens on surfaces without the need for an active antimicrobial. If the coatings were made from heat conducting materials, they may find applications in heat transfer enhancement. Finally, there are many consumer surfaces, such as on car exteriors and bathrooms, where it might be desirable for droplets to evaporate quickly. An advantage of a coating is that it can be simply added to various devices to give new utility rather than changing the bulk material of the devices.

Author contributions.

CRediT authorship contribution statement

Mohsen Hosseini: Conceptualization, Data curation, Formal analysis, Investigation, Methodology, Writing – original draft, Writing – review & editing. **Alejandro Rodriguez:** Writing – original draft, Formal analysis. **William A. Ducker:** Conceptualization, Project administration, Methodology, Formal analysis, Resources, Supervision, Writing – review & editing.

Data availability

Data will be made available on request.

Declaration of Competing Interest

The authors declare that they have no known competing financial interests or personal relationships that could have appeared to influence the work reported in this paper.

Acknowledgements

This work was performed in part at the Nanoscale Characterization and Fabrication Laboratory, which is supported by the Virginia Tech National Center for Earth and Environmental Nanotechnology Infrastructure (NanoEarth), a member of the National Nanotechnology Coordinated Infrastructure (NNCI), supported by NSF (ECCS 1542100 and ECCS 2025151). This work was supported by the National Science Foundation under Grant No. CBET-1902364.

Appendix A. Supplementary material

Supplementary data to this article can be found online at https://doi.org/10.1016/j.jcis.2022.11.065.

References

[1] O. Amer, R. Boukhanouf, H.G. Ibrahim, A review of evaporative cooling technologies, Int. J. Environ. Sci. Develop. 6 (2) (2015) 111–117.
[2] Y. Yang, G. Cui, C.Q. Lan, Developments in evaporative cooling and enhanced evaporative cooling-A review, Renew. Sustain. Energy Rev. 113 (2019), https://doi.org/10.1016/j.rser.2019.06.037 109230.
[3] A.-H. Cavusoglu, X. Chen, P. Gentine, O. Sahin, Potential for natural evaporation as a reliable renewable energy resource, Nat. Commun. 8 (1) (2017) 1–9, https://doi.org/10.1038/s41467-017-00581-w.
[4] A. Abd El-Rahman Elsayed Saad, C. Aydemir, S. Ayhan Özsoy, S. Yenidoğan, Drying methods of the printing inks, Journal of Graphic Engineering and Design 12 (2) (2021) 29–37.
[5] T. Suganthi, P. Senthilkumar, Moisture-management properties of bi-layer knitted fabrics for sportswear, J. Ind. Text. 47 (7) (2018) 1447–1463, https://doi.org/10.1177/1528083717692594.
[6] M. Hosseini, S. Behzadinasab, Z. Benmamoun, W.A. Ducker, The viability of SARS-CoV-2 on solid surfaces, Curr. Opin. Colloid Interface Sci. 55 (2021), https://doi.org/10.1016/j.cocis.2021.101481 101481.
[7] M. Hosseini, A.W.H. Chin, S. Behzadinasab, L.L.M. Poon, W.A. Ducker, Cupric Oxide Coating That Rapidly Reduces Infection by SARS-CoV-2 via Solids, ACS Appl. Mater. Interfaces 13 (5) (2021) 5919–5928, https://doi.org/10.1021/acsami.0c19465.
[8] M. Hosseini, S. Behzadinasab, A.W.H. Chin, L.L.M. Poon, W.A. Ducker, Reduction of Infectivity of SARS-CoV-2 by Zinc Oxide Coatings, ACS Biomater Sci. Eng. 7 (11) (2021) 5022–5027, https://doi.org/10.1021/acsbiomaterials.1c01076.
[9] A. Jiao, R. Riegler, H. Ma, G. Peterson, Thin film evaporation effect on heat transport capability in a grooved heat pipe, Microfluid. Nanofluid. 1 (3) (2005) 227–233, https://doi.org/10.1007/s10404-004-0015-6.
[10] R. Mandel, M. Ohadi, A. Shooshtari, S. Dessiatoun, Thin film evaporation on microstructured surfaces—Application to cooling high heat flux electronics, 2011 27th Annual IEEE Semiconductor Thermal Measurement and Management Symposium, IEEE, 2011, pp. 138-145.
[11] C. Sodtke, P. Stephan, Spray cooling on micro structured surfaces, Int. J. Heat Mass Transf. 50 (19–20) (2007) 4089–4097, https://doi.org/10.1016/j.ijheatmasstransfer.2006.12.037.
[12] T. Metzger, A. Irawan, E. Tsotsas, Influence of pore structure on drying kinetics: A pore network study, AIChE J 53 (12) (2007) 3029–3041, https://doi.org/10.1002/aic.11307.
[13] N. Unno, K. Yuki, R. Inoue, Y. Kogo, J. Taniguchi, S.-i. Satake, Enhanced evaporation of porous materials with micropores and high porosity, Journal of Thermal Science and Technology 15(1) (2020) JTST0007-JTST0007 doi:10.1299/jtst.2020jtst0007.
[14] R. Gimenez, G.J. Soler-Illia, C.L.A. Berli, M.G. Bellino, Nanopore-Enhanced Drop Evaporation: When Cooler or More Saline Water Droplets Evaporate Faster, ACS Nano 14 (3) (2020) 2702–2708, https://doi.org/10.1021/acsnano.9b06618.
[15] M. Goncalves, J.Y. Kim, Y. Kim, N. Rubab, N. Jung, T. Asai, S. Hong, B.M. Weon, Droplet evaporation on porous fabric materials, Sci. Rep. 12 (1) (2022) 1087, https://doi.org/10.1038/s41598-022-04877-w.
[16] A. Oko, P. Claesson, A. Swerin, Imbibition and evaporation of water droplets on paper and solid substrates, Journal of Imaging Science and Technology 55(1) (2011) 10201-1-10201-6 doi:10.2352/J.ImagingSci.Technol.2011.55.1.010201.
[17] A. Oko, D.M. Martinez, A. Swerin, Infiltration and dimensional scaling of inkjet droplets on thick isotropic porous materials, Microfluid. Nanofluid. 17 (2) (2014) 413–422, https://doi.org/10.1007/s10404-013-1313-7.
[18] F. Canbazoglu, B. Fan, A. Kargar, K. Vemuri, P. Bandaru, Enhanced solar evaporation of water from porous media, through capillary mediated forces and surface treatment, AIP Adv. 6 (8) (2016), https://doi.org/10.1063/1.4961945 085218.
[19] J.Y.H. Goh, Y.M. Hung, M.K. Tan, Extraordinarily enhanced evaporation of water droplets on graphene-nanostructured coated surfaces, Int. J. Heat Mass Transf. 163 (2020), https://doi.org/10.1016/j.ijheatmasstransfer.2020.120396 120396.
[20] W. Li Tong, W.-J. Ong, S.-P. Chai, M.K. Tan, Y. Mun Hung, Enhanced evaporation strength through fast water permeation in graphene-oxide deposition, Sci. Rep. 5 (1) (2015) 1–13, https://doi.org/10.1038/srep11896.
[21] M. Hanlon, H. Ma, Evaporation heat transfer in sintered porous media, J. Heat Transfer 125 (4) (2003) 644–652, https://doi.org/10.1115/1.1560145.
[22] J. Plawsky, A. Fedorov, S. Garimella, H. Ma, S. Maroo, L. Chen, Y. Nam, Nano-and microstructures for thin-film evaporation—a review, Nanoscale Microscale

Thermophys. Eng. 18 (3) (2014) 251–269, https://doi.org/10.1080/15567265.2013.878419.
[23] T.A. Nguyen, A.V. Nguyen, Increased evaporation kinetics of sessile droplets by using nanoparticles, Langmuir 28 (49) (2012) 16725–16728, https://doi.org/10.1021/la303293w.
[24] Y. Bo-Ming, Fractal character for tortuous streamtubes in porous media, Chin. Phys. Lett. 22 (1) (2005) 158, https://doi.org/10.1088/0256-307X/22/1/045.
[25] J. Cai, B. Yu, A discussion of the effect of tortuosity on the capillary imbibition in porous media, Transp. Porous Media 89 (2) (2011) 251–263, https://doi.org/10.1007/s11242-011-9767-0.
[26] C. Jian-Chao, Y. Bo-Ming, M. Mao-Fei, L. Liang, Capillary rise in a single tortuous capillary, Chin. Phys. Lett. 27 (5) (2010), https://doi.org/10.1088/0256-307X/27/5/054701 054701.
[27] B. Yu, J. Li, Some fractal characters of porous media, Fractals 9 (03) (2001) 365–372, https://doi.org/10.1142/S0218348X01000804.
[28] H. Hu, R.G. Larson, Evaporation of a sessile droplet on a substrate, J. Phys. Chem. B 106 (6) (2002) 1334–1344, https://doi.org/10.1021/jp0118322.
[29] R.D. Deegan, O. Bakajin, T.F. Dupont, G. Huber, S.R. Nagel, T.A. Witten, Contact line deposits in an evaporating drop, Phys. Rev. E 62 (1) (2000) 756, https://doi.org/10.1103/PhysRevE.62.756.
[30] M. Hosseini, L.L.M. Poon, A.W.H. Chin, W.A. Ducker, Effect of Surface Porosity on SARS-CoV-2 Fomite Infectivity, ACS Omega 7 (22) (2022) 18238–18246, https://doi.org/10.1021/acsomega.1c06880.